Article

Applied Spectroscopy

Applied Spectroscopy
2019, Vol. 73(10) 1160–1171

DOI: 10.1177/0003702819868237
journals.sagepub.com/home/asp
SAGE

Spatial Heterodyne Raman Spectrometer (SHRS) for In Situ Chemical Sensing Using Sapphire and Silica Optical Fiber Raman Probes

Joshua M. Ottaway[1], Ashley Allen[2], Abigail Waldron[2], Phillip H. Paul[1], S. Michael Angel[2], and J. Chance Carter[1]

Abstract

A spatial heterodyne Raman spectrometer (SHRS), constructed using a modular optical cage and lens tube system, is described for use with a commercial silica and a custom single-crystal (SC) sapphire fiber Raman probe. The utility of these fiber-coupled SHRS chemical sensors is demonstrated using 532 nm laser excitation for acquiring Raman measurements of solid (sulfur) and liquid (cyclohexane) Raman standards as well as real-world, plastic-bonded explosives (PBX) comprising 1,3,5- triamino- 2,4,6- trinitrobenzene (TATB) and octahydro-1,3,5,7-tetranitro-1,3,5,7-tetrazocine (HMX) energetic materials. The SHRS is a fixed grating-based dispersive interferometer equipped with an array detector. Each Raman spectrum was extracted from its corresponding fringe image (i.e., interferogram) using a Fourier transform method. Raman measurements were acquired with the SHRS Littrow wavelength set at the laser excitation wavelength over a spectral range of ~1750 cm^{-1} with a spectral resolution of ~8 cm^{-1} for sapphire and ~10 cm^{-1} for silica fiber probes. The large aperture of the SHRS allows much larger fiber diameters to be used without degrading spectral resolution as demonstrated with the larger sapphire collection fiber diameter (330 μm) compared to the silica fiber (100 μm). Unlike the dual silica fiber Raman probe, the dual sapphire fiber Raman probe did not include filtering at the fiber probe tip nearest the sample. Even so, SC sapphire fiber probe measurements produced less background than silica fibers allowing Raman measurements as close as ~85 cm^{-1} to the excitation laser. Despite the short lengths of sapphire fiber used to construct the sapphire probe, well-defined, sharp sapphire Raman bands at 420, 580, and 750 cm^{-1} were observed in the SHRS spectra of cyclohexane and the highly fluorescent HMX-based PBX. SHRS measurements of the latter produced low background interference in the extracted Raman spectrum because the broad band fluorescence (i.e., a direct current, or DC, component) does not contribute to the interferogram intensity (i.e., the alternating current, or AC, component). SHRS spectral resolution, throughput, and signal-to-noise ratio are also discussed along with the merits of using sapphire Raman bands as internal performance references and as internal wavelength calibration standards in Raman measurements.

Keywords

Raman spectroscopy, spatial heterodyne Raman spectrometer, Fourier transform Raman, FT Raman, optical fiber, Raman probe, sapphire fiber, PBX, TATB, HMX

Date received: 9 February 2019; accepted: 27 June 2019

Introduction

Beginning in the late 1990s, and subsequently fueled by the Food and Drug Administration's process analysis technologies in the pharmaceutical industry initiative,[1–3] there was a significant increase in the use of Raman spectroscopy, particularly in the area of industrial process analysis,[4] that has continued to grow to the present day. For many process applications, optical fiber Raman probes are a key enabler for transitioning from off-line to real-time and in situ,

[1]Lawrence Livermore National Laboratory, Livermore, CA, USA
[2]Department of Chemistry and Biochemistry, University of South Carolina, Columbia, SC, USA

Corresponding author:
J. Chance Carter, Lawrence Livermore National Laboratory, 7000 East Avenue, Livermore, CA 94550-5507, USA.
Email: carter45@llnl.gov

on-line, or in-line sample analysis. The evidence for this can be found in the introduction of new application driven (e.g., liquids and transparent solids, turbid liquids, solid powders, gases/vapors) commercial Raman probes and turnkey fiber-coupled Raman spectrographs (i.e., slit and grating-based spectrometer equipped with an array detector) along with new competitors in this market space.

The vast majority of commercial optical fiber Raman probes are fabricated using industry standard, high-purity, clad silica fibers that provide low-loss transmission in the spectral regions, near ultraviolet (UV) to near-infrared (NIR), where Raman instruments operate, small diameter (cores range from single to hundreds of microns) sizes to interface with Raman spectrographs, chemical inertness with high melting points for operation in harsh environments, and high tensile strength and mechanical flexibility for measurements over long lengths of fiber or in confined spaces. Commercial-off-the-shelf (COTS) silica/silica-doped clad fibers are available with numerical apertures (NA) of 0.12, 0.22, and 0.26, although custom optical fiber options are available along with higher NA options,[5] if polymer-based claddings are used. Given the limited choices of COTS fiber NAs for probe fabrication, the spectrograph etendue should be designed or adapted (*f*-number and area matching) to equal or exceed that of the fiber probe. Optical filtering is also critical for fiber probes fabricated using silica fibers since the Raman spectrum of the amorphous silica fiber contains broad interference features and luminescence[6] that extend from the lowest frequency region to $\sim$1300 cm^{-1} depending on the dopant used in the silica cladding.[7] Laser delivery fibers with narrow bandpass filters centered at the excitation wavelength block the silica Raman scattering from exiting the fiber, and collection fibers with long pass filters reject scattered laser light; both filter types are ideally positioned and affixed between the fiber ends and the sample.[8]

For probe designs using separate fibers for laser delivery and backscattered light collection, the laser intensity delivered to a given sample and Raman scattering intensity for a given sample is primarily determined by the location of and degree of overlap between the light illumination cone of the excitation fiber and the field-of-view cone of the collection fiber(s).[9] In operation, Raman scattered light is transmitted via the collection fiber(s) to the entrance aperture of the spectrograph where light is dispersed onto the charge-coupled device (CCD) detector. The spectral resolution and range depend on several parameters including the entrance aperture (slit) width, the linear dispersion (i.e., spectrograph focal length and grating angular dispersion), and the CCD array pixel size. In the case of fiber-coupled Raman spectrographs, collection fiber(s) can serve as the input aperture by imaging or physically positioning the fiber(s) at the focal plane of the slit; if a probe comprises multiple collection fibers, these must be arranged in a linear geometry ($1 \times n$; $n =$ # of fibers) parallel to the slit height dimension. Whether single or multiple collection fibers are used, the *f*-number of the spectrograph should also equal the fiber *f*-number to maximize throughput. Because the spectral resolution and throughput of Raman spectrographs are strongly interconnected parameters, increasing the collection fiber(s) diameter with a corresponding increase in the slit width increases etendue but reduces the spectral resolution.

Unlike Raman spectrographs, the heterodyne approach of the recently demonstrated spatial heterodyne Raman spectrometer (SHRS),[10] a fixed grating-based dispersive interferometer equipped with an array detector, has only a weak coupling of spectral resolution and throughput, enabling a large input aperture and wide acceptance angle ($\sim 1^\circ$ or $\sim 10^\circ$ using field widening prisms) and diffraction limited spectral resolution (i.e., equal to the resolving power of the combined diffraction gratings), resulting in high light throughput and a much larger field of view of the interrogated sample and simultaneously high spectral resolution. Thus, the SHRS can provide high spectral resolution with much higher throughput than a similar sized Raman spectrograph. The SHRS follows the fixed-grating interferometer design first proposed by Connes[11] and later modernized by Harlander[12–14] in which constructive and destructive interference of incoming light produces a two-dimensional Fizeau pattern of fringes (i.e., interferogram) that is imaged onto an array detector and used to extract spectral information via Fourier transform methods[15]; a combination of beamsplitter and two fixed diffraction gratings are typically used, but a slit is not required. The lack of a slit and the resulting large etendue has several important implications for designing new Raman probes for use with the SHRS. Much larger diameter optical fibers can be used to fabricate probes with no loss of spectral resolution, and the multifiber interface to the SHRS does not require a linear ($1 \times n$) arrangement. Fiber probes can also incorporate higher NA fibers including photonic crystal, hollow core, liquid core, and single-crystal fibers.

For select fiber-based Raman sensor applications, single-crystal (SC) fibers such as sapphire (Al_2O_3) have physical and optical properties that offer important advantages. Compared to silica fibers, the sapphire fiber SC structure produces relatively sharp Raman features observed at $\sim$425, 580, and 750 cm^{-1} when excited and measured within the fiber. These features, which are consistent with other reports,[16–18] can serve as internal performance references and wavelength calibration standards while minimally affecting the Raman spectra of most samples, similar to what has been shown for other fibers.[19,20] Raman probes fabricated using SC sapphire fibers can deliver very high laser energies (>1 J/pulse)[21] to the sample, which could be useful for Raman measurements involving pulsed laser

excitation and samples with high damage thresholds. Unclad sapphire also has a higher melting temperature (~2000 °C) than silica fiber (~1400 °C) and is mechanically stronger although somewhat stiffer (7 × higher Young's modulus)[21] and therefore less flexible. Sapphire fibers are produced by different growth methods[22] in lengths ranging from ~3 to 5 m depending on fiber diameter, which is a limitation for many Raman applications, and any cladding must be added after the fibers are grown.[23] Still, SC sapphire Raman probes have many potential uses including embedded sensing in harsh or inaccessible environments and applications requiring high power laser, pulsed or continuous wave (CW), delivery.

In this work, we evaluate and compare the performance of the SHRS with a spectrally filtered, lensed silica fiber Raman probe and a custom unfiltered, non-lensed, SC sapphire probe. To the best knowledge of the authors, this is the first demonstration of an SHRS chemical sensor using optical fiber Raman probes, which differs from other reports[24,25] involving the use of silica fibers only for light collection. The utility of the fiber-coupled SHRS chemical sensor is demonstrated using 532 nm excitation for measuring a variety of solid and liquid Raman standards and real-world samples of high explosive (HE) formulations while simultaneously characterizing spectral resolution, throughput, and signal-to-noise ratio (SNR).

Experimental

SHRS Setup

All Raman measurements unless noted in the text were acquired using an SHRS, comprising three subsystems (see Fig. 1): Imager, Interferometer, and Illuminator. The latter subsystem interfaces directly to the Raman probe collection fiber and includes an achromatic lens (Thorlabs ac127-019-A-ML) and multiple filters (Omega Optical, shortpass, RPE630SP; Semrock, longpass, LP03-532RE-25; Kaiser Optical, SuperNotch laser rejection, HS-532). The Interferometer is designed with two stationary diffraction gratings (Richardson grating model 33009FL01-201R; 25 mm square, 150 grooves/mm; 500 nm; 2.2° blaze angle) and a cube beamsplitter (Thorlabs, BS016, 20 mm; $T_{abs} = 57\%$, $R_{abs} = 43\%$ at 532 nm). A zero-aperture adjustable iris diaphragm (Thorlabs, SM1D12SZ) having a maximum opening of 12 mm was positioned between each

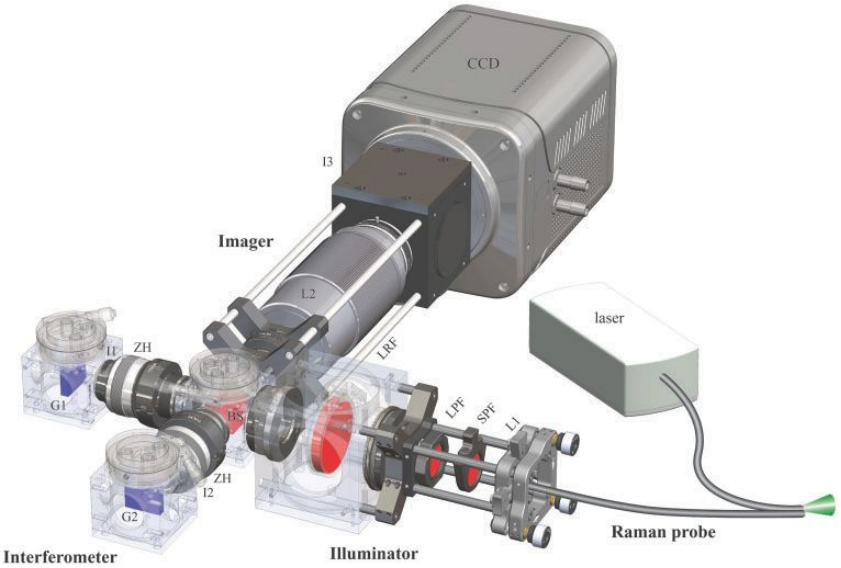

Figure 1. A spatial heterodyne Raman spectrometer (SHRS) comprising the Imager, Interferometer, and Illuminator subsystems is illustrated along with a two-fiber Raman probe, which interfaces to the laser source and Illuminator. One fiber delivers laser light to the sample, while the other fiber collects and delivers the resulting Raman scattered light to the Illuminator where the light is collimated (L1) and spectrally filtered via shortpass (SPF), longpass (LPF), and laser rejection filters (LRF). The light then enters the Interferometer where it is divided at the beamsplitter (BS) into two beams with a fixed phase relationship (i.e., coherent) and directed toward gratings (G1, G2) that diffract the light at wavelength dependent angles back toward the beamsplitter where the light is recombined, producing an interferogram that is imaged onto the CCD via a camera lens (L2). The SHRS is designed with irises (I1, I2) for manually blocking light to either grating and for (I3) blocking unwanted grating diffraction orders (second order and above at the CCD entrance aperture). A non-rotating zoom housing (ZH) positioned between each grating (G1, G2) and the beamsplitter enables adjustment of the working distance of either grating with respect to the beamsplitter without rotating the grating.

grating and the beamsplitter. A low-power diode laser (Thorlabs, CPS532, 532 nm) was used to set the Interferometer Littrow wavelength.

The interferogram (i.e., fringe Fizeau pattern) along with other images used in postprocessing are digitally recorded by the Imager comprising a camera lens (Coastal Optical Systems, Inc., 105 mm, *f*/4 UV-MICRO-APO, 111032) and a frame transfer, electron multiplier (EM) CCD array detector (Princeton Instruments, ProEM-HS:1024BX3, 1024 × 1024–13.5 μm square pixels), which is oriented, so the readout direction of the image is parallel to the vertically aligned fringe pattern. The camera lens was positioned 254 mm from the detector and 203 mm from the gratings for $m = 1.25$ magnification.[†] An adjustable iris diaphragm (Thorlabs, SM2D25) with a maximum opening of 25 mm was positioned between the lens and CCD. All CCD images were acquired with LightField (Princeton Instruments, v.6) software at the following settings: non-EM, high gain/low noise mode; 100 kHz or 1 MHz analog-to-digital conversion readout speeds; maximum spatial resolution (i.e., no vertical or horizontal binning); and −70 °C thermoelectric cooling with additional water cooling. The optional CCD air-cooling fan was deactivated in the LightField software.

A CW, frequency-doubled Nd:YAG laser (Spectra-Physics, Millennia eV5S, 532 nm, <60 GHz line width) was used as the excitation source for all SHRS measurements. Using the manufacturer's graphical user interface to control the laser, the minimum output power of 500 mW was selected and attenuated external to the laser head using a combination half-wave plate and polarizer (Thorlabs, WPH05M-532; GT10-A).

Two types of optical fiber probes, each having a separate excitation delivery and collection fiber, were used for performing SHRS measurements: first, a commercially available lensed, holographic-filtered Raman probe (Kaiser Optical Systems, Mark II, HFPH-FC-S-532). The Mark II probe is a well-known single excitation/single collection optical fiber Raman probe with a spectral coverage that enables Raman measurements starting at 100 cm^{-1}, per the manufacturer's specification. In the Kaiser probe, excitation radiation is delivered to the sample through a 1 m long, 50 μm diameter silica optical fiber and focused onto the sample with an attached Olympus 10 × microscope objective lens having a 6 mm focal length. Raman scattering is then collected by the same microscope objective in backscatter (180° geometry) and relayed to the SHRS through a second 1 m long, 100 μm diameter silica optical fiber.

Second, as a proof-of-concept demonstration, a custom sapphire probe comprising two unclad SC sapphire optical fibers (330 μm diameter, ~20 mm length, ~1.74 refractive index, $NA_{eff} \cong 0.35$ in air[23]) was assembled (see Fig. 1) by adjacently positioning and securing the distal ends (i.e., the sensing end) of each fiber while minimizing contact along the fiber lengths. At the distal end, the sapphire collection fiber was recessed by 1 mm from the sapphire laser delivery fiber, and unlike the Kaiser probe, no optics or filtering was used between the distal sapphire fiber ends and the sample.

SHRS Operation

Referring to Fig. 1, light from a narrow-band laser source is coupled into an optical fiber and delivered to the distal end of the Raman probe where the sample is excited. Spontaneous Raman scattered light is collected by a different fiber and transmitted to the SHRS Illuminator subsystem where it is collimated and spectrally and sometimes spatially filtered before entering the Interferometer. Within the Interferometer, the collimated light is divided at the beamsplitter into two beams with a fixed phase relationship (i.e., coherent) and with preferably equal power, that are directed toward tilted gratings of equal distance spacing from the beamsplitter and having identical groove densities, *d*. As described by Eq. 1, the *n*th order light at wavelength λ (nm) and incident on the grating at angle α is diffracted by the grating at angle β and directed back toward the beamsplitter where the light is recombined with that returned from the other grating; the assumption here is that all optical components are positioned along the same optical axis. The combined light produces an interferogram (i.e., a Fizeau fringe pattern) that is reconstructed by the camera lens of the Imager and digitally recorded on the array detector. The lens is positioned to image the grating onto the detector. The optimal focus is critical for achieving the theoretical spectral bandpass, which is seldom realized. The Raman spectrum is extracted by taking a Fourier transform of the postprocessed interferogram as described in more detail in the next section

$$n\lambda = d(\sin\alpha + \sin\beta) \tag{1}$$

Both Interferometer gratings are tilted (i.e., tilted from normal incidence and parallel to the dispersion planes of the gratings) to the Littrow angle (θ_L) as described by Eq. 2. At this angle, there is a corresponding wavelength known as the Littrow wavelength (λ_L) where the light traverses from the beamsplitter to both gratings and back to the beamsplitter along an identical optical path ($\alpha = \beta$ for Eq. 1) resulting in no light interference. The Littrow wavelength is the corresponding reference about which the interferogram is heterodyned

$$\theta_L = \sin^{-1}\frac{n\lambda_L}{2d} \tag{2}$$

All wavelengths other than the Littrow wavelength traverse a different angular optical path producing crossing wavefronts of light that result in a wavelength dependent two-dimensional interference pattern of fringes having a spatial frequency defined by

$$f = 4(\sigma - \sigma_L)\tan\theta_L \tag{3}$$

where f is in units of fringes/cm, σ is the wavenumber (cm^{-1}) of the Raman spectral feature, σ_L is the Littrow wavelength in units of wavenumbers (cm^{-1}), and θ_L is the Littrow angle. For all SHRS measurements presented herein, the Littrow wavelength was set very near the laser excitation wavelength of 532 nm by adjusting the tilt angle of both gratings in first order by $\sim 2.3^\circ$ (according to Eq. 2). When the Littrow wavelength is set very near the laser excitation wavelength, the heterodyne part of Eq. 3, $(\sigma - \sigma_L)$, is equivalent to Raman shift (RS). The maximum value of RS, also known as the spectral bandpass, that can be measured for a given SHRS setup is given by Eq. 4

$$\mathrm{RS} \leq \frac{N\sigma_L}{2R} \tag{4}$$

where N is the number of pixels illuminated on the array detector, σ_L is the Littrow wavelength, and R is the resolving power of the SHRS. For the SHRS Kaiser fiber probe setup with a 1944 resolving power and 600 pixels illuminated on the CCD, the spectral bandpass at the laser excitation wavelength of 532 nm is 2900 cm^{-1}.

SHRS Image Processing

Four CCD images were collected for each sample measured: a raw interferogram image, an image of each grating (performed by blocking the other grating), and an image of the beamsplitter (performed by blocking both gratings). Data post processing including SHRS image corrections, image region-of-interest (ROI) selection, and Fourier transforms were performed using custom codes written for Matlab software (The MathWorks Inc., v2017b). All SHRS interferogram images were postprocessed as follows to produce what is referred to in the text as the corrected image: the images of each individual grating, which included the beamsplitter in both, were subtracted from the raw interferogram image, and a single image of the beamsplitter only was added back to the raw image. Using the corrected image, a circular ROI capturing only the area illuminated on the CCD was selected with remaining pixels set to zero (i.e., zero filling) to preserve a 1024 by 1024 image size. The Fourier transform was applied to each individual row[15] of the corrected image using Matlab's built in fast Fourier transform (FFT) function. The absolute value of each row was used to remove the imaginary component of the FFT, and all rows were then summed to produce the final Raman spectrum.

SHRS Sample Preparation

Samples of cyclohexane (Fisher Scientific, C556-1) and sulfur (JT Baker, #4088) were used for characterizing the SHRS and for comparing the silica and sapphire probes. The sublimed sulfur powder was pressed into a wafer using a 13 mm pellet die (Carver, catalog #3619). Liquid measurements were conducted using 10 mm and 1 mm pathlength quartz cuvettes (Hellma, 111-10-40 and 110-1-40). In addition, two real-world HE formulations based on octahydro-1,3,5,7-tetranitro-1,3,5,7-tetrazocine (HMX) and 1,3,5-triamino-2,4,6-trinitrobenzene (TATB) were tested. Plastic-bonded explosive (PBX) molding powder (also known as "prill") was supplied by the High Explosives Applications Facility (HEAF) at Lawrence Livermore National Laboratory. The powder particles are aggregates of HE and a polymer binder. The formulations investigated in this study also included a nitroplasticizer or dye. In addition to the formulated PBXs, pure binder materials and one of the dyes were also obtained from HEAF. The PBX formulations investigated in this study are shown in Table I. Approximately 10 mg of the powder was loaded in a cylindrical die and pressed for three minutes at room temperature using a 30 ton press with a hand pump (ENERPAC, Model P-392) connected to the hydraulic ram cylinder (ENERPAC, Model RC-59). The powder was not evacuated prior to pressing. In-die pressure was 30 000 psi. The resulting solid wafer weighed approximately 10 mg and had dimensions of approximately 3.14 mm diameter by 0.67 mm thickness. Density was at least 95% theoretical maximum density (1.94 and 1.86 g/cm^3 for LX-17-1 and PBX-9501, respectively).[26] The pressed wafers were physically robust, showing no visible evidence of breaking, chipping, or cracking.

Results and Discussion

SHRS–Raman Probe Measurements of Raman Standards

SHRS–Raman probe measurements were acquired with Raman standards using the commercial Kaiser silica fiber and custom SC sapphire fiber Raman probes. Figures 2a and 2b show the corrected images (i.e., interferograms),

Table I. PBX formulations.

PBX	HE	Binder	Plasticizer	Dye
LX-17-1	92.5% TATB	7.5% Kel-F 800	None	Polyester Dark Red FL
PBX 9501	95% HMX	2.5% Estane 5703	2.5% BDNPA-F	None

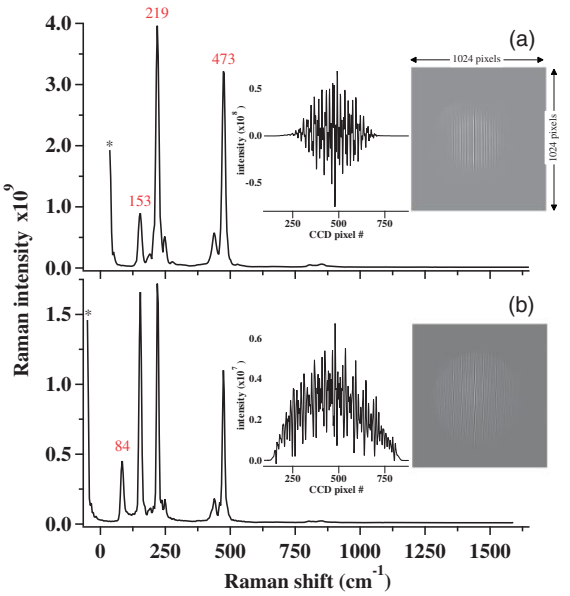

Figure 2. Interferogram corrected images, image cross-sections, and corresponding Raman spectra of a pressed sulfur wafer were acquired with 100 mW of 532 nm CW laser excitation and 60 s integration times using (a) silica and (b) sapphire optical fiber Raman probes with the SHRS (see Fig. 1). For these measurements the SHRS heterodyne wavelength was set very near the laser excitation wavelength.

image cross-sections, and corresponding Raman spectra of sulfur collected with the Kaiser and sapphire probes, respectively, using the same SHRS. Each Raman spectrum was extracted from its corresponding CCD interferogram corrected image (Fig. 2 insets) using a Fourier transform method[15] and plotted as Raman scattering intensity versus wavenumber. The Raman bands for sulfur corresponding to 85, 153, 219, and 473 cm^{-1} are observed in the SHRS sapphire (unfiltered) probe measurements (Fig. 2b), whereas the 532 nm holographic laser rejection filters in the SHRS Kaiser silica probe completely block the 85 cm^{-1} band and attenuate the 153.8 cm^{-1} Raman band (Fig. 2a); the remaining Raman bands were not affected. Even though an intensity calibration was not performed to account for the SHRS instrument response, the relative intensities of the Raman bands are approximately correct for sulfur. The factor of two decrease in Raman signal intensity for the SHRS sapphire probe measurement is attributed in part to disruption of the total internal reflection in the unclad sapphire fibers as the excitation and collection fibers are brought together and physically touch to form the distal sensor tip. This only affected the Raman intensity collected and transmitted to the SHRS because the same laser power (100 mW) at the sample was used for all SC sapphire and Kaiser probe comparison measurements. Only the Raman Stokes shifted spectral regions are observed in these spectra; to prevent overlap of wavenumbers above (Stokes) and below (anti-Stokes) the Littrow wavelength of 18 796 cm^{-1} (532 nm) as described by Eq. 3 and previously reported,[10] a 532 nm longpass filter was placed in the SHRS Illuminator's collimated light path to remove anti-Stokes Raman.

When optimally collimated, the Kaiser Raman probe collection fiber (100 μm diameter) produces a calculated (CCD interferogram image: 600 pixel diameter × 0.0135 mm $pixel^{-1}$/1.25 Imager magnification) 6.48 mm illuminated spot on each grating, resulting in a maximum theoretical resolving power, *R*, of 1944 (2 grating 6.48 mm/grating × 150 grooves per mm). The calculated spectral resolution of the Kaiser probe coupled SHRS is ~10 cm^{-1} (18 797 cm^{-1}/1944). Likewise, the sapphire collection fiber (330 μm diameter) produces a calculated spot of 7.84 mm on each grating, resulting in a maximum theoretical resolving power of 2352; the calculated spectral resolution for the sapphire probe SHRS is ~8 cm^{-1}. Ray trace analysis (not shown) was performed to aid in selecting an Illuminator lens with an appropriate focal length for use with either fiber diameter for mitigating light clipping by the lens and at the zero-aperture adjustable iris—the limiting aperture in the SHRS optical path. Even so, some minor clipping at the iris was observed for all sapphire fiber measurements, which is attributed to less than perfect hand polishing of the sapphire fiber ends. A comparison of the corrected image cross-sections in Fig. 2 provides evidence of a slight misalignment resulting in non-optimal overlap of the light diffracted by the gratings when using the sapphire fiber. In Fig. 2b, the cross-section of the corrected image for the sapphire probe measurement shows the interferogram atop a broad intensity band of light that was not accounted for in the background subtractions used to produce the corrected image. In Fig. 2a, the cross-section of the corrected image for the Kaiser silica probe measurement is mostly symmetric about the *x*-axis at zero intensity, indicating better alignment of the fiber, beamsplitter and gratings and illumination overlap in the Interferometer.

The prominent features labeled with an asterisk (*) and located at the first pixel position in Figs. 2a and 2b Raman spectra of sulfur is similarly present in all Raman spectra presented in this paper and a direct result of the FFT post-processing used to extract the Raman spectrum from the corrected image. Any non-Raman scattered light (e.g., fluorescence, ambient, any light outside the SHRS spectral bandpass, etc.) that produces a broad intensity band across the array detector will not produce resolvable fringes in the interferogram. Likewise, grating misalignments may result in a Littrow wavelength mismatch that does not produce observable fringes. As a result, the FFT leads to the observable systematic artifact positioned at the zero position (first, DC component pixel position). Importantly, all broad band sources still contribute to shot noise in the Raman spectrum even though these do not show up in the Raman spectrum itself, and the noise at all wavelengths is distributed equally throughout the spectrum.

Commercial silica-based probes such as the Kaiser probe are designed for use at a specific laser excitation wavelength owing to the type of filters used between the fiber and the sample for wavelength rejection. The transmission profile of the filter(s), which is angle dependent, along with the magnitude of Rayleigh scatter attenuation are critical factors that determine how close Raman bands can be measured relative to the laser excitation wavelength. Kaiser probes typically utilize holographic filtering with several orders of magnitude Rayleigh attenuation and a sharp spectral cutoff that optimally enables measurements starting at 100 cm^{-1}. The Raman spectrum in Fig. 2b shows a cutoff > 100 cm^{-1}, which indicates non-optimal performance near the excitation wavelength. In some cases, this slight redshift can be corrected by adjusting the angle of the filter(s) to regain the 100 cm^{-1} factory specification. However, the redshift observed for the Kaiser probe used in these studies is not related to an optical alignment issue but rather attributed to a progressing redshift in the filter itself[‡] that is not correctable by adjusting the filter angle. The only spectral region affected by the slight redshift in the transmission of the probe profile is very near the laser excitation wavelength.

Unlike the Kaiser probe and most other commercial Raman probes, the custom sapphire fiber Raman probe is not restricted to a single excitation wavelength and can utilize much higher laser powers compared to similar sized probes since there are no filters between the fiber ends and the sample. In miniature silica-based Raman probe designs where very small filters (e.g., few 100 μm diameter sized) are attached to the ends of fibers, the amount of laser power delivered to the sample is often limited due to light absorption and subsequent heating that can affect filters and the epoxies often used to affix filters to the polished ends of fibers. Finally, filters in the optical train are different from probe-to-probe and must be calibrated out and assumed to not vary in application. That the sapphire fiber probe can avoid using these filters between the fiber ends and sample provides the ability to detect small shifts and serves to improve method transferability (by reducing or removing the systematic error incurred in making filter transmission corrections).

Figures 3a and 3b show the extracted Raman spectra of cyclohexane acquired at a laser excitation power of 100 mW with the Kaiser and sapphire probes, respectively, using the SHRS. The previously reported[27,28] Raman bands for cyclohexane corresponding to 384, 426, 802, 1029, 1158, 1267, and 1443 cm^{-1} are observed in both Fig. 3 spectra, while the weakest Raman band at 1347 cm^{-1} is only observed in Fig. 3a spectrum owing to the ~sixfold higher SNR. Figure 3b spectrum includes two additional Raman bands at 425 and 750 cm^{-1} attributed to Raman scattering from the probe's sapphire fibers (see Fig. 3b inset). The intensity of the sapphire fiber Raman bands is low because of the short lengths of fiber used in this study. The intensity could be increased

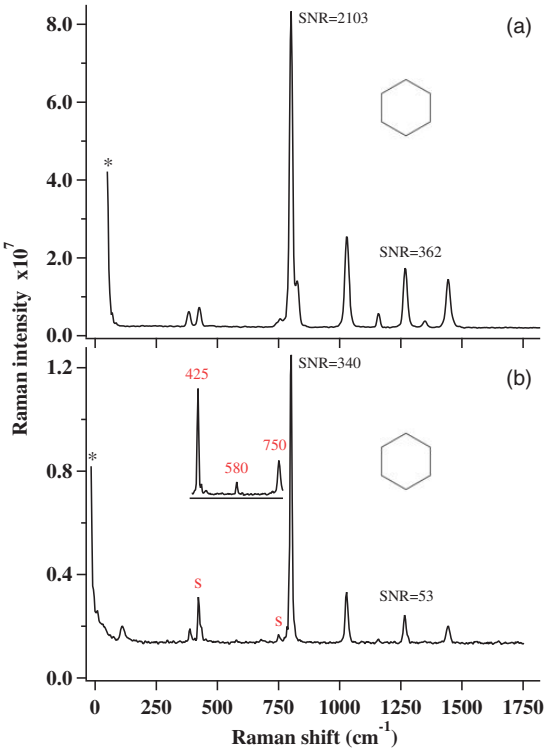

Figure 3. Raman spectra of cyclohexane were acquired with 100 mW of 532 nm CW laser excitation and 60 s integration times using (a) silica and (b) sapphire optical fiber Raman probes with the SHRS (see Fig. 1) heterodyne wavelength set very near the laser excitation wavelength. Spectrum in (b) clearly shows sapphire Raman bands(s) at 425 and 750 cm^{1}, one of which overlaps with the cyclohexane Raman band at 426 cm^{-1}. The inset in (b) is the Raman spectrum of the sapphire fiber itself. Note: No silica Raman was observed in the spectrum of cyclohexane acquired with the silica fiber Raman probe.

using longer fibers if desired, for use as an internal wavelength calibration reference.

For measurements performed with the SHRS Kaiser probe, a microscope objective attached to the probe focused the laser beam to the center of a 10 mm cuvette filled with neat cyclohexane. For measurements with the dual-fiber flat tip sapphire probe, a 1 mm cuvette was used. Even though the cuvette pathlengths differ by a factor of 10, in the case of the Kaiser probe, the collection volume is mainly constrained to the focal region of the probe's microscope objective. For this reason, focused fiber Raman probes are useful for acquiring in situ Raman measurements through glass and plastic sample containers[29] without significant signal contribution from the sample container.

Unlike the Kaiser probe, a lens was not used for SC sapphire probe measurements. Rather, the sapphire fibers were arranged as a dual-fiber flat tipped probe with the unclad distal fiber ends adjacently secured and physically touching. At this minimal (300 μm) center-to-center fiber separation, the Raman probe sensitivity is highest within

a few millimeters from the fiber tips where overlap of the excitation and collection fibers' field of view (i.e., Raman interrogation volume) is maximum.[9] In terms of the light emitting and gathering capability, the unclad SC sapphire fibers have a refractive index of ~1.74 and an $NA_{eff} \cong 0.35$ in air,[23] while the Kaiser's silica fibers have an NA of 0.26. The *f*/# of the sapphire and silica collection fibers are 1.43 ($f/\# = 1/\{2 \times NA\}$) and 1.92, respectively, which means the sapphire fiber has the capability to gather ~1.8 times more light, resulting in increased Raman sensitivity. However, given the crude construction of the proof-of-demonstration SC sapphire probe, the overall Raman sensitivity is far from optimized and even less so for very short path length (<1 mm) measurements of transparent liquids such as cyclohexane.

SHRS–Raman Probe Measurements of Real-World Samples

Plastic-bonded explosives (PBXs), also called polymer-bonded explosives, were first developed in 1952, and have since become very important for a variety of commercial and national security applications. PBXs comprise the explosive and binder and may include a plasticizer and a dye for ease of identification. The plastic (e.g., polymer) coating that binds the explosive granules, typically 5% to 20% of each formulation by weight, is what gives each PBX its distinctive characteristics in terms of energetic content, mechanical properties, safety and chemical stability.[30] Given the growing interest in monitoring PBXs and other energetic materials remotely and in situ using nondestructive methods, two safe and stable PBX formulations (see Table 1) based on octahydro-1,3,5,7-tetranitro-1,3,5,7-tetrazocine (HMX) and 1,3,5-triamino-2,4,6-trinitrobenzene (TATB) HEs were selected for testing with the fiber-coupled SHRS.

As shown in Figs. 4a and 4b, SHRS measurements of PBX 9501 were acquired using the Kaiser Optical silica fiber and sapphire fiber probes, respectively, and processed as previously described to extract the Raman spectrum from the corrected image. Except for the non-Raman spectral artifact (*) located at the zero-wavelength position, all bands in Fig. 4a are Raman bands of HMX. Similarly, Fig. 4b spectrum includes the same spectral features in addition to low-frequency HMX Raman bands (96, 139, 149, 181 cm^{-1}) and sapphire Raman bands (425, 580, 750 cm^{-1}), which overlap to varying degrees with HMX bands. As previously

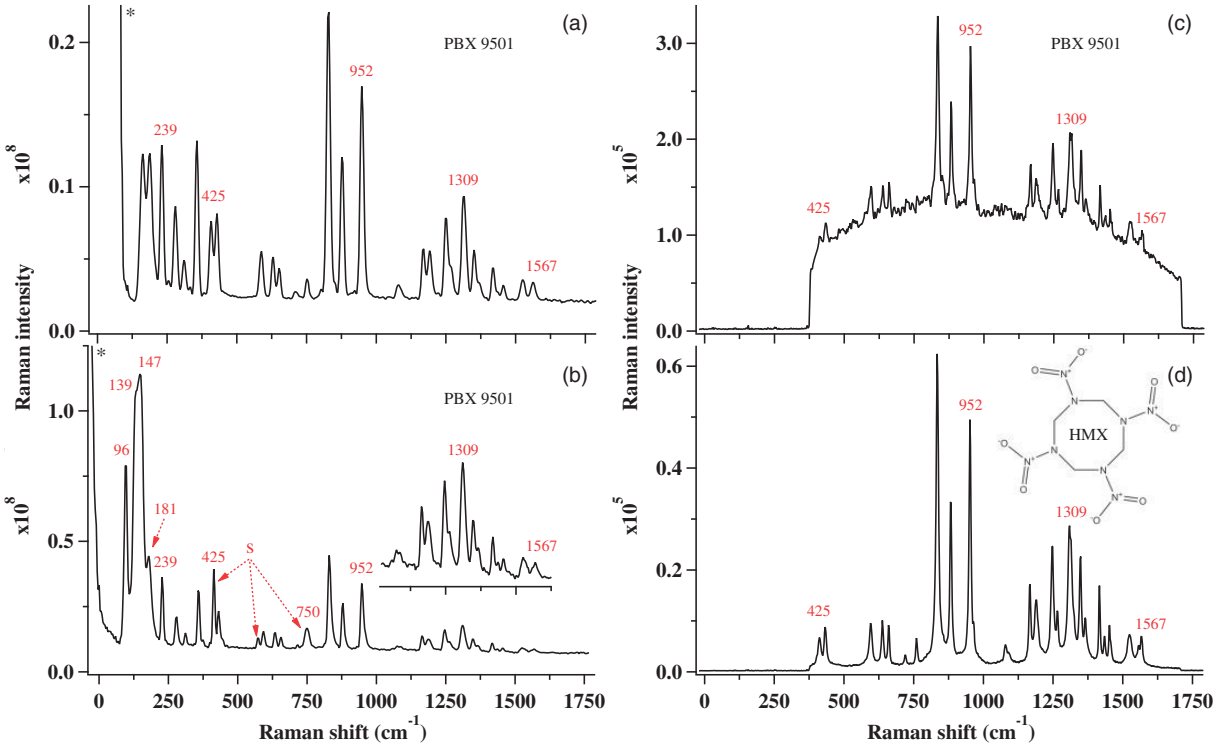

Figure 4. Raman spectra of the HMX-based plastic-bonded explosive formulation, PBX 9501, were acquired with 100 mW of 532 nm CW laser excitation and 60 s integration times using (a) silica and (b) sapphire optical fiber Raman probes with the SHRS (see Fig. 1) heterodyne wavelength set very near the laser excitation wavelength. For comparison, the figure also shows the Raman spectrum of (c) PBX 9501 and the (d) HMX explosive component measured with a conventional Raman spectrograph and a fiber Raman probe at 785 nm laser excitation. Note: The Raman spectrum of PBX 9501 is dominated by HMX Raman bands with no discernable spectral features from the other formulation components other than fluorescence.

discussed, the holographic laser rejection filters in the SHRS Kaiser silica probe attenuates spectral features below ~220 cm^{-1} and completely blocks the lowest frequency Raman bands.

Exhibiting significant fluorescence when excited with 532 nm laser excitation, the typical broadband background of PBX 9501 commonly observed with Raman spectrograph measurements of fluorescent samples (see Fig. 4c) is not observed in Figs. 4a and 4b SHRS spectra. With the SHRS, broad band luminescence does not produce resolvable fringes in the interferogram, resulting in the spectral artifact (*) at the zero-wavelength (i.e., DC component) position when the data is transformed using the FFT. For qualitatively comparing backgrounds, Fig. 4c Raman spectrum of PBX 9501 was acquired at 785 nm laser excitation using a (silica) fiber-coupled Raman spectrograph (Kaiser Optical Systems, Holospec *f*/1.8i with attached 785 nm Mark II probe, HFPH-FC-S-785) equipped with an intensified CCD array detector; the intensifier dimensions limited the spectral range of the measurement rather than filtering in the Raman probe. Compared to shorter, visible wavelengths (e.g., 532 nm), Raman measurements using laser excitation at NIR wavelengths can significantly reduce fluorescence. Figure 4c Raman bands, which are also attributed to HMX, are observed atop a broad intense background of fluorescence. (Note: The baseline noise in Figs. 4a and 4b should not be compared with Fig. 4c since the noise is distributed differently in the SHRS and spectrograph instruments.) Furthermore, the use of an intensified CCD (ICCD) operating in non-gated mode at –30 °C is typically noisier and less sensitive than a deeply cooled, back thinned CCD, which was not available at the time.

As shown in Fig. 4d, the Raman spectrum of HMX powder was also acquired using the fiber-coupled Raman spectrograph at 785 nm excitation. When compared to Fig. 4c, the relatively low observed fluorescence background indicates the source of fluorescence in PBX 9501 is the polymer binder and plasticizer and not the HE material. This was confirmed via Raman measurements of the individual pure component binder and plasticizer (not shown). Figure 4d spectrum, along with Sharma et al.,[31] confirms that the Raman spectrum of PBX 9501 is dominated by HMX Raman bands with no discernable spectral features of the polymer binder and plasticizer other than fluorescence. The relative intensities of Raman bands in Figs. 4a and 4b are also different from those of Figs. 4c and 4d.

Figures 5a and 5b show the Raman spectrum of LX-17-1 and TATB powder acquired with the Kaiser probe coupled SHRS (532 nm excitation) and a fiber-coupled Raman spectrograph (785 nm excitation), respectively. The Raman band with a peak at 386 cm^{-1} is partially clipped in Fig. 5b spectrum owing to the more limited spectral range with the ICCD setup. The 14 prominent Raman bands (less prominent at 292 cm^{-1} and from ~1375 to 1630 cm^{-1}) observed in Fig. 5a spectrum are assigned to the TATB component in

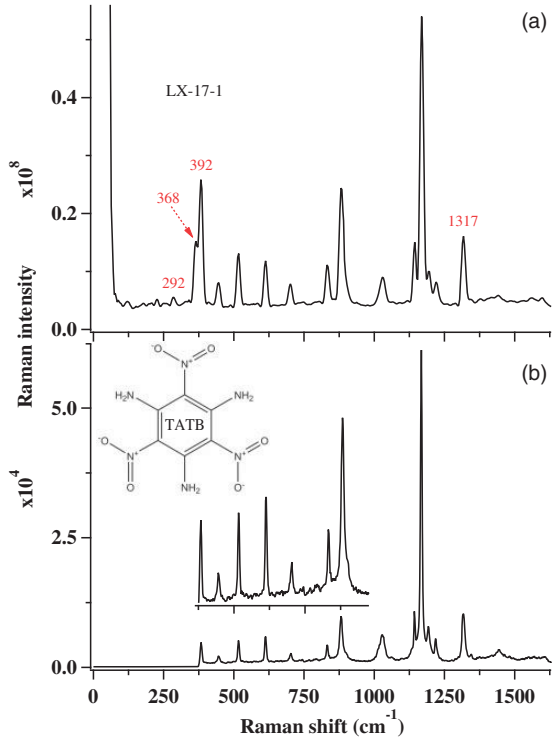

Figure 5. The Raman spectrum of (a) TATB-based plastic-bonded explosive formulation, LX-17-1, was acquired with 2.5 mW of 532 nm CW laser excitation and a 60 s integration time using the silica fiber Raman probe with the SHRS (see Fig. 1) heterodyne wavelength set very near the laser excitation wavelength. For comparison, panel (b) shows the Raman spectrum of the TATB explosive component only measured with a conventional Raman spectrograph and attached fiber Raman probe at 785 nm laser excitation. The inset of (b) is an expanded view of the spectral range from ~375 to 975 cm^{-1}. Note: The Raman spectrum of LX-17-1 is dominated by TATB Raman bands with no discernable spectral features from the other formulation components.

the LX-17-1 formulation; the Raman scattering of TATB powder (Fig. 5b) and the other LX-17-1 pure components (not shown) were individually measured to confirm these assignments. Furthermore, the band assignments and relative Raman intensities for the SHRS measurements are consistent with previously reported[31] TATB powder Raman spectra acquired with a Raman spectrograph at 532 nm excitation. Spectral features below 292 cm^{-1} are difficult to discern given the baseline noise and expected signal attenuation from laser rejection filtering in the Kaiser probe.

Although not fully investigated as part of these studies, the differences in relative band intensities between the Raman spectra measured using 532 (Fig. 5a) and 785 nm (Fig. 5b) is likely due, at least in part, to suspected 532 nm absorption by the yellowish TATB component and the polymer binder and dye. In fact, very low laser power (~3 mW) measurements at 532 nm excitation produced

higher signal-to-noise Raman spectra compared to higher laser power measurements. At these low laser powers, no evidence of photo and/or thermal sample degradation was observed although photochemical effects have been observed with UV excitation.[32] The instrument response functions, which were not measured and corrected using intensity calibrations, is another contributor to the relative band intensity differences. Moreover, it has been reported that the SHRS system response decreases at wavelengths far from Littrow.[33,34]

Frame Transfer CCD Detection with the SHRS

For the first time, an SHRS designed with a frame transfer CCD has been demonstrated as a viable alternative to full frame CCDs with image intensifiers or mechanical shutters. The motivation for using a frame transfer CCD was driven by the unique, integrated design of the SHRS system illustrated in Fig. 1, which utilizes modular optical cage and lens tube systems. This design directly connects the Interferometer subsystem, the most vibration sensitive part of the SHRS, to the Illuminator and Imager subsystems. The frame transfer CCD does not utilize a mechanical shutter, which has the potential to introduce vibrations upon opening and closing during image acquisitions. Furthermore, the frame transfer CCD used in these studies can operate at $-70\,^{\circ}C$ with water cooling instead of an air-cooling fan, which also has the potential to produce vibrations. (Note: All prior reported SHRS systems have utilized free-space optical designs where the Interferometer subsystem is not physically attached to the other subsystems except where mounted to a common optical table or breadboard.)

Frame transfer devices utilize a parallel architecture in which half the detector array is used for imaging and the other half for storage; the storage array is physically masked to block incoming light. The imaging array collects image data, which is then rapidly transferred to the storage array where it can be exported via the CCD electronics. Generally speaking, the advantage of frame transfer is faster data acquisition, which could be important for some measurements but not those presented herein. The downside to frame transfer is image smearing, which can occur since light is constantly impinging upon the imaging array during the transfer. Provided any smearing is within the noise of the measurement, this is of little consequence. For SHRS measurements, the fine fringe structure corresponding to spectral features located far from the Littrow wavelength are likely the most affected by any image smearing. This has the potential to degrade fringe visibility and spectral resolution and limit the overall spectral range of the measurement. Despite these concerns, no such effects were observed in any of the fiber-coupled SHRS measurements presented in this paper. It is also worth noting that we recently substituted the frame transfer CCD with a full frame CCD (Princeton Instruments, PIXIS 2048B; 13.5 μm pixel, 2 MHz) operating with a mechanical shutter and cooling fan and successfully acquired fiber-coupled SHRS data of various Raman standards without issue. Additional follow-on studies are planned.

Conclusion

This study describes the first demonstration of an SHRS using optical fiber Raman probes. In situ, SHRS measurements of inorganic and organic compounds including PBXs of HMX and TATB were successfully demonstrated using Raman probes constructed from all silica and all SC sapphire optical fibers. The overall quality of SHRS data acquired under the same experimental conditions using either probe is very good and similar. The sapphire Raman probe was constructed using 330 μm diameter fibers, which did not degrade the SHRS spectral resolution owing to the large acceptance angle of the SHRS. The sapphire probe also did not utilize optical filters between the probe tip and sample, yet the fiber background is lower than the filtered silica fiber probe; Raman bands within 85 cm^{-1} of the laser line were measured for sulfur using the sapphire fiber Raman probe. Although there was some overlap with analyte Raman bands, the sharp, well-defined Raman bands from the sapphire fibers did not prevent analyte identification.

Furthermore, these sapphire bands are potentially useful as an internal standard for wavelength and might also be useful as a performance reference for the overall SHRS system. It was also observed that highly fluorescent samples such as the HMX-based PBX could be measured with the SHRS with little background interference because the DC component of the broad band fluorescence does not contribute to the interferogram intensity (i.e., AC component).

The overall results from this work demonstrate the utility of the SHRS for real-world sample analyses of liquids and solids using optical fiber probes. Although PBXs were a focus of this paper, the technique is amenable to other families of HEs including melt-cast, liquid, and cast cure. The robustness, low background and built-in calibration would make SC sapphire fiber Raman probes useful for industrial process applications requiring real-time, in situ measurements.

Acknowledgments

This work was performed under the auspices of the U.S. Department of Energy by Lawrence Livermore National Laboratory under Contract DE-ac52-07NA27344.This document was prepared as an account of work sponsored by an agency of the United States government. Neither the United States government nor Lawrence Livermore National Security, LLC, nor any of their employees makes any warranty, expressed or implied, or assumes any legal liability or responsibility for the accuracy, completeness, or usefulness of any information, apparatus, product, or process disclosed, or represents that its use would not infringe

privately owned rights. Reference herein to any specific commercial product, process, or service by trade name, trademark, manufacturer, or otherwise does not necessarily constitute or imply its endorsement, recommendation, or favoring by the United States government or Lawrence Livermore National Security, LLC. The views and opinions of authors expressed herein do not necessarily state or reflect those of the United States government or Lawrence Livermore National Security, LLC, and shall not be used for advertising or product endorsement purposes.

It is with great sadness that this public acknowledgment comes a year after the passing of Professor James A. Harrington, formerly of the Materials, Science and Engineering Department at Rutgers University, who generously provided the sapphire fibers used in this study. Among his many accomplishments, Professor Harrington was a pioneer in the field of specialty fiber optics and infrared optical materials.

Conflict of Interest

The authors declared no potential conflicts of interest with respect to the research, authorship, and/or publication of this article.

Funding

The Angel Group at USC would like to thank the National Science Foundation (Awards CHE-1308211 and OCE-1829333) and NASA (grant no. NNX14AI34G and 80NSSC19K1024) for supporting the work at The University of South Carolina.

Notes

† The thin lens law provides $1/f = 1/s + 1/s'$, where the distances to object and image, s and s', respectively, are measured from the two principal planes of the camera lens. These two planes are separated by a thickness p that is a property of the lens. The distance between object and image is then $w = s + p + s' = p + f\,(2 + m + 1/m)$, where $m = s'/s$ is the magnification (image to object) and $f = 105$ mm is the focal length of the lens. The lens was used to image an object on the bench, and the magnification at a given image-to-object distance was recorded. Application of the derived relationship provides the measurement, $p = 32$ mm. In the instrument, the grating-to-detector separation was measured at 457 mm, using the measured value for p and the derived relationship gives a magnification for the instrument of 1.25.

‡ There is a known issue that can affect some but not all one-inch holographic notch filters that comprise Kaiser Mark II probes. The onset of a redshift in the transmission profile is thought to develop once the protective glass seal of the filter is breached by ambient conditions; this is a random occurrence that can affect relatively new or old Kaiser probes. Once the redshift starts it can eventually progress to the point where the filters no longer block the excitation wavelength for which the probe was designed. The fix for this issue is replacement of the filter(s). The Kaiser probe utilized in these studies was manufactured in August 2016. The observed redshift shown herein represents an early onset of the redshift in the transmission profile, which only affects the spectral region very near the laser excitation wavelength.

References

1. U.S. Department of Health and Human Services, Food and Drug Administration. "PAT–A Framework for Innovative Pharmaceutical Development, Manufacturing, and Quality Assurance: Guidance for Industry". 2004. https://www.fda.gov/regulatory-information/search-fda-guidance-documents/pat-framework-innovative-pharmaceutical-development-manufacturing-and-quality-assurance [accessed Jul 17 2019].
2. H. Wikstrom, I.R. Lewis, L.S. Taylor. "Comparison of Sampling Techniques for In-Line Monitoring Using Raman Spectroscopy". Appl. Spectrosc. 2005. 59(7): 934–941.
3. D.C. Hinz. "Process Analytical Technologies in the Pharmaceutical Industry: The FDA's PAT Initiative". Anal. Bioanal. Chem. 2006. 384: 1036–1042.
4. I.R. Lewis. "Process Raman Spectroscopy". In: I.R. Lewis, H.G.M. Edwards, editors. Handbook of Raman Spectroscopy. New York: Marcel Dekker Inc., 2001. Chap. 23, p.919.
5. B.J. Skutnik, B. Foley, K.B. Moran. "High-Numerical-Aperture Silica Core Fibers". Proc. SPIE. 2004. 5317: 39–45.
6. M.L. Myrick, S.M. Angel, R. Desiderio. "Comparison of Some Fiber Optic Configurations for Measurement of Luminescence and Raman Scattering". Appl. Opt. 1990. 29(9): 1333–1344.
7. G.E. Walrafen, J. Stone. "Raman Spectral Characterization of Pure and Doped Fused Silica Optical Fibers". Appl. Spectrosc. 1975. 29(4): 337–344.
8. J. Ma, Y.-S. Li. "Fiber Raman Background Study and Its Application in Setting up Optical Fiber Raman Probes". Appl. Opt. 1996. 35(15): 2527–2533.
9. T.F. Cooney, H.T. Skinner, S.M. Angel. "Comparative Study of Some Fiber-Optic Remote Raman Probe Designs. Part I: Model for Liquids and Transparent Solids". Appl. Spectrosc. 1996. 50(7): 836–848.
10. N.R. Gomer, C.M. Gordon, P. Lucey, et al. "Raman Spectroscopy Using a Spatial Heterodyne Spectrometer: Proof of Concept". Appl. Spectrosc. 2011. 65(8): 849–857.
11. P.P. Connes. "Spectromètre Interférentiel a Sèlection par L'Amplitude de Modulation". J. Phys. Radium. 1958. 19(3): 215–222.
12. J.M. Harlander. Spatial Heterodyne Spectroscopy: Interferometric Performance at Any Wavelength Without Scanning. [Doctoral Dissertation]. Madison, Wisconsin: The University of Wisconsin, 1991.
13. J. Harlander, R.J. Reynolds, F.L. Roesler. "Spatial Heterodyne Spectroscopy for the Exploration of Diffuse Interstellar Emission Lines at Far-Ultraviolet Wavelengths". Astrophys. J. 1992. 396: 730–740.
14. J.M. Harlander, F.L. Roesler, S. Chakrabarti. "Spatial Heterodyne Spectroscopy: A Novel Interferometric Technique for the FUV". Proc. SPIE. 1990. 1344: 120–131.
15. P.D. Barnett, K.A. Strange, S.M. Angel. "Improving Spectral Results Using Row-by-Row Fourier Transform of Spatial Heterodyne Raman Spectrometer Interferogram". Appl. Spectrosc. 2017. 71(6): 1380–1386.
16. T. Wermelinger, C. Borgia, C. Solenthaler, et al. "3-D Raman Spectroscopy measurements of the Symmetry of Residual Stress Fields in Plastically Deformed Sapphire Crystals". Acta Mater. 2007. 55: 4657–4665.
17. C. Raml, X. He, M. Han, et al. "Raman Spectroscopy Based on a Single-Crystal Sapphire Fiber". Opt. Lett. 2011. 36(7): 1287–1289.
18. B. Liu, Z. Yu, Z. Tian, et al. "Temperature Dependence of Sapphire Fiber Raman Scattering". Opt. Lett. 2015. 40(9): 2041–2044.
19. P.I. Okagbare, M.D. Morris. "Fluorocarbon Fiber-Optic Raman Probe for Non-Invasive Raman Spectroscopy". Appl. Spectrosc. 2012. 66(6): 728–730.
20. D. Pristinski, H. Du. "Solid-Core Photonic Crystal Fiber as a Raman Spectroscopy Platform with a Silica Core as an Internal Reference". Opt. Lett. 2006. 31(22): 3246–3248.

21. R.K. Nubling, J.A. Harrington. "Optical Properties of Single-Crystal Sapphire Fibers". Appl. Opt. 1997. 36(24): 5934–5940.
22. J.A. Harrington. "Single-Crystal Fiber Optics: a Review". Proc. SPIE. 2014. 8959: 895902-1–895902-9.
23. R.K. Nubling, R.L. Kozodoy, J.A. Harrington. "Optical Properties of Clad and Unclad Sapphire Fiber". Proc. SPIE. 1994. 2131: 56–61.
24. N.R. Gomer, M.P. Nelson, S.M Angel. "The Development of a Wide-Field, High-Resolution UV Raman Hyperspectral Imager". Chemical, Biological, Radiological, Nuclear, Explosives (CBRNE) Sensing XVI. Proc. SPIE. 2015. 9455: 94550N-1–94550N-8.
25. M.J. Foster, J. Storey, M.A. Zentile. "Spatial-Heterodyne Spectrometer for Transmission-Raman Observations". Opt. Express. 2017. 25(2): 1598–1604.
26. B.M. Dobratz, P.C. Crawford. LLNL Explosives Handbook: Properties of Chemical Explosives and Explosive Simulants. Tech. Rep. UCRL-52997 Change 2. Livermore, CA: Lawrence Livermore National Laboratory, 1985.
27. F.A. Miller, H.R. Golob. "The Infrared and Raman Spectra of Cyclohexane and Cyclohexane-d_{12}". Spectrochim. Acta, Part A. 1964. 20(10): 1517–1530.
28. K.B. Wiberg, A. Shrake. "A Vibrational Study of Cyclohexane and Some of its Isotopic Derivates – I: Raman and Infrared Spectra and Assignments of Cyclohexane and Cyclohexane-d_{12}". Spectrochim. Acta, Part A. 1971. 27(7): 1139–1151.
29. J.C. Carter, W.E. Brewer, S.M. Angel. "Raman Spectroscopy for the In Situ Identification of Cocaine and Selected Adulterants". Appl. Spectrosc. 2005. 54(12): 1876–1881.
30. A.W. Lundberg. "High Explosives in Stockpile Surveillance Indicate Constancy". Sci. Technol. Rev. 1996. 1201: 12–17.
31. S.K. Sharma, A.K. Misra, B. Sharma. "Portable Remote Raman System for Monitoring Hydrocarbon, Gas Hydrates and Explosives in the Environment". Spectrochim. Acta, Part A. 2005. 61(10): 2404–2412.
32. A.D. Britt, W.B. Moniz, G.C. Chingas, et al. "Free Radicales of TATB". Propellants Explos. 1981. 6(4): 94–95.
33. N. Lamsal, S.M. Angel. "Deep-Ultraviolet Raman Measurements Using a Spatial Heterodyne Raman Spectrometer". Appl. Spectrosc. 2015. 69(5): 525–534.
34. N. Lamsal, S.K. Sharma, T.E. Acosta, et al. "Ultraviolet Stand-off Raman Measurements Using a Gated Spatial Heterodyne Raman Spectrometer". Appl. Spectrosc. 2016. 70(4): 666–675.